2008

Estimation of Submarine Groundwater Discharge from Bulk Ground Electrical Conductivity Measurements

Thomas Stieglitz

John Rapaglia
Sacred Heart University, rapagliaj@sacredheart.edu

Henry Bokuniewicz

Recommended Citation

Stieglitz, T., J. Rapaglia, and H. Bokuniewicz. "Estimation of submarine groundwater discharge from bulk ground electrical conductivity measurements." Journal of Geophysical Research (2008) 113:C08007.

Estimation of submarine groundwater discharge from bulk ground electrical conductivity measurements

Thomas Stieglitz,[1,2] John Rapaglia,[3] and Henry Bokuniewicz[3]

Received 10 August 2007; revised 13 February 2008; accepted 27 February 2008; published 6 August 2008.

[1] The utility of bulk ground conductivity (BGC) measurements in the estimation of submarine groundwater discharge (SGD) was investigated at four sites covering a range of hydrogeological settings, namely Cockburn Sound (Australia); Shelter Island (USA); Ubatuba Bay (Brazil) and Flic-en-Flac Bay (Mauritius). At each of the sites, BGC was surveyed in the intertidal zone, and seepage meters were used for direct measurements of SGD flow rates. In the presence of detectable salinity gradients in the sediment, a negative correlation between SGD and BGC was recorded. The correlation is site-specific and is dependent on both the type of sediment and the mixing processes. For example, at Shelter Island the maximum mean flow rates were 65 cm d^{-1} at a BGC of $\sim$0 mS cm^{-1} while at Mauritius maximum mean flow rates were 364 cm d^{-1} at a BGC of $\sim$0 mS cm^{-1}. BGC measurements are used to estimate SGD over a large scale, and to separate its fresh and saline components. Extrapolating BGC measurements throughout the study sites yields a total discharge of 2.91, 1.59, 7.16, and 25.4 10^3 m^3 d^{-1} km^{-1} of shoreline with a freshwater fraction of 41, 24, 29, and 63% at Cockburn Sound, Shelter Island, Ubatuba Bay, and Flic-en-Flac Bay respectively. The results demonstrate that ground conductivity is a useful tracer to survey and separate freshwater and recirculated seawater component of SGD. The presented investigation is a subset within a series of experiments designed to compare different methods to investigate SGD co-organized and carried out by SCOR, LOICZ, IOC and IAEA.

Citation: Stieglitz, T., J. Rapaglia, and H. Bokuniewicz (2008), Estimation of submarine groundwater discharge from bulk ground electrical conductivity measurements, *J. Geophys. Res.*, *113*, C08007, doi:10.1029/2007JC004499.

1. Introduction

[2] Submarine groundwater discharge (SGD) is recognized as an important component in the water balance, water quality, and the ecology of many coastal areas [e.g., *Johannes*, 1980; *Crusius et al.*, 2005; *Kaleris*, 2005; *Mulligan and Charette*, 2006; *Moore*, 2006; *Schiavo et al.*, 2006; *Beck et al.*, 2007]. Studies of SGD are often limited by uncertainty in both accurately quantifying flow rates as well as separating the terrestrial and marine components of SGD [*Burnett et al.*, 2001; *Taniguchi et al.*, 2002; *Taniguchi and Iwakawa*, 2004; *Crusius et al.*, 2005; *Burnett and Dulaiova*, 2006]. SGD has been shown to be highly variable on both spatial scales and timescales [*Bokuniewicz et al.*, 2003; *Paulsen et al.*, 2004; *Rapaglia*, 2005; *Burnett et al.*, 2006; *Stieglitz et al.*, 2007]. Although the use of tracers for integrated measurements over large areas, and mathematical models based on traditional hydrogeologic parameters are commonly used, direct point measurements using vented, benthic chambers, known as seepage meters, remain a primary tool for the direct measurement of SGD [*Lee*, 1977; *Bokuniewicz*, 1980; *Taniguchi and Fukuo*, 1993; *Bokuniewicz et al.*, 2003; *Paulsen et al.*, 2004; *Taniguchi et al.*, 2005; *Taniguchi*, 2006]. Where flow patterns are inhomogeneous, however, chamber measurements can only be considered representative of the small part of the seafloor which they cover, and their utility for estimation of total flux into, e.g., an embayment, may be compromised. A combination of different measuring techniques, both integrated and direct, may complement one another to better constrain SGD measurements [*Burnett et al.*, 2006]. Here we summarize investigations of the utility of (electrical) ground conductivity measurements as a tool for the quantification of SGD, especially in interpolating and extrapolating point measurements across larger areas, and determining the relative contribution of fresh and marine groundwaters.

[3] While SGD has been successfully located, mapped and/or quantified with various water column tracers including salinity [e.g., *Milham and Howes*, 1994], relatively few studies have used pore water salinity or ground conductivity as a means of determining the location and rate of SGD. Where terrestrially derived fresh or brackish groundwater is of interest, salinity and conductivity can be used as a tracer. Ground conductivity (also referred to as apparent bulk conductivity) is a function of porosity and salinity of the

[1]School of Maths, Physics and IT, James Cook University, Townsville, QLD, Australia.
[2]Australian Institute of Marine Science, Townsville, QLD, Australia.
[3]Marine Sciences Research Center, Stony Brook University, Stony Book, New York, USA.

0148-0227/08/2007JC004499

interstitial water. Direct measurement of pore water salinity profiles have been utilized to study this relationship without the uncertainty associated with the formation factor and other sediment properties [*Martin et al.*, 2007]. Pore water sample extraction however can be laborious and time-consuming. We suggest that as an alternative, ground conductivity which can be very rapidly measured, can be used under certain conditions in place of pore water salinity measurements to gain a better estimate of SGD flux. With this method, larger area can be surveyed in a significantly shorter period of time than can be achieved with pore water sampling. In this paper, we explore the use of a rapid method of surveying bulk ground conductivity along transects to improve total SGD flux estimates from an area calculated from point flux measurements.

[4] However, BGC is a function of both the pore water salinity and the pore space [e.g., *Kermabon et al.*, 1969]. Both an increase in the salinity of the interstitial water or porosity will result in an increase in BGC. This needs to be accounted for by a formation factor, as will be introduced in the methods section. In practice, variations of pore water salinity are significantly greater than variations of porosity (or pore water fraction), and it is this relationship that can be used in studies of fresh SGD. In previous work, a number of different sensor designs have been employed to measure conductivity, or its inverse, resistivity. *Kermabon et al.* [1969] used a heavy electrode array inserted into deep sea sediments off the coast of Sicily to relate the conductivity of the groundwater brine to the conductivity of the saturated sands. *Lee* [1985] used a towed conductivity sensor to identify anomalies in bottom/sediment conductivity. *Vanek and Lee* [1991] used a combination of the aforementioned conductivity probe, a pore water sampler, and bulk ground conductivity measurements to map potential zones of fresh groundwater discharge in Sweden.

[5] Further work on the use of bulk ground conductivity patterns as a proxy for fresh SGD has been attempted at several sites in which the use of an in situ conductivity probe inserted into the sediment was employed [*Stieglitz et al.*, 2000, 2007; *Stieglitz*, 2005]. Using this method, sediment was measured in which BGC was significantly reduced near pockmarks called "wonky holes" on the Great Barrier Reef Shelf [*Stieglitz*, 2005], and SGD from unconfined and confined shallow aquifers into the coastal zone was mapped [*Stieglitz*, 2005]. The same conductivity sensor was employed in the study presented here.

[6] Mapping SGD by streaming conductivity surveys was reported by *Manheim et al.* [2004a, 2004b], in which streamer cables were towed behind a boat in transects across coastal bays of the Delmarva Peninsula. The investigators report high quality results when trying to locate areas of fresh groundwater discharge along transects of 8 to 30 km in length. Low conductivity zones from tens of meters to several kilometers in length were discriminated from high conductivity regions elsewhere. *Breier et al.* [2005] compared resistivity measurements along a 17 km transect near Corpus Christi, Texas against radium measurements. A region of low sediment conductivity (<8 mS cm^{-1}) in the center of the bay corresponded to high water column radium, suggesting a discharge of fresher groundwater in the zone. *Swarzenski et al.* [2006] used a high resolution 56 electrode resistivity cable to create a time series of images of the subsurface sediment conductivity at Dor Beach, Israel. These images were able to clearly reproduce the hydrogeological patterns pending water level variations. An estimated first-order water exchange determined from the time series compared well with measurements of SGD made by quantifying the ^{222}Rn input into the system. Meanwhile, *Swarzenski et al.* [2007] used the same resistivity cable in a shore-perpendicular array to measure the impact of tidal variation on the coastal aquifer in Hood Canal, Washington. They found that the, up to 5 m, tidal amplitude can cause decimeter scale changes to the local coastal aquifer, which were compared with ^{222}Rn in the local waters. A strong inverse correlation was seen between the coastal aquifer head and the 222Rn concentration of the surface water.

2. Methods

2.1. Conductivity Survey

[7] Conductivity was recorded in situ using a high resolution conductivity probe, consisting of four ring electrodes (2 cm diameter) configured in a Wenner array with a vertical electrode spacing of 1 cm [*Stieglitz et al.*, 2000]. The ratio of current to induced voltage is proportional to ground conductivity. Vertical conductivity profiles were recorded by inserting the probe into the ground, taking a reading at a particular depth, and then successively pushing the probe further into the ground. At each site a series of transects were surveyed in which measurements were taken several meters apart, with higher spatial resolution in areas with significant conductivity gradients. Measurements were taken at depth intervals of 10 cm to a maximum depth of 1 m to 1.5 m below the sediment interface. At each depth, the probe was left in place until readings stabilized. Transect data were interpolated by kriging using SURFER 6.0, taking spatial anisotropy in data points into account. When low BGC (<3 mS cm^{-1}) is found in saturated sediment, the assumption is made that there is a significant presence of fresh interstitial water. If BGC is higher than this value, there must be some conducting salts in the sediment. Typically, data along a transect of a length of tens of meters is collected within 30 to 45 min.

2.2. Interpretation of Conductivity Measurements

[8] The ratio of current to induced voltage measured with the sensor is proportional to bulk ground conductivity (σ_b) and is typically measured in milli-Siemens per centimeter of linear distance (mS cm^{-1}). BGC is a function of current-inducing salts in the sediment and is based both on the conductivity (σ_w) of the pore water and any conductive contribution of the solid sediment matrix [e.g., *Kermabon et al.*, 1969; *Urish*, 1981; *Stieglitz*, 2005]. Pore water conductivity depends on the salinity and the temperature of the pore water. A temperature conversion can be applied relative to a reference temperature, T_{ref}, as

$$\sigma_T = \sigma_{ref}(T + 21.4)/(T_{ref} + 21.4) \quad (1)$$

[9] Some investigators have used resistivity (proportional to the inverse of conductivity) measurements to locate areas of high discharge. Bulk ground resistivity (ρ_B) can be converted to pore water resistivity (ρ_w) using a formation factor, F, as: $\rho_w = F\ \rho_B$ [*Manheim et al.*, 2004a]. The

formation factor, F is based on a combination of porosity, Φ, according to Archie's Law (e.g., *Telford et al.* [1990] as cited by *Zhou et al.* [2000]) and the sediment's tortuosity [*Kermabon et al.*, 1969; *Ullman and Aller*, 1982]. The tortuosity is a measure of the distance a particle of water must travel to get through a porous layer, and can be defined by the ratio on the specific surface of the porous medium to that of the idealized capillary bundle [*Saripalli et al.*, 2003].

$$F = \phi^{-m} \tag{2}$$

where m is an empirical constant determined with values between 1.2 and 4 based on tortuosity as well as a reasonable bulk resistivity measurement, which is dependent on temperature and soil moisture [*Kermabon et al.*, 1969; *Ullman and Aller*, 1982; *Maerki et al.*, 2004]. Resistivity (units of ohm-meter) can then be converted to conductivity (σ_w, mS cm^{-1}) by the relationship

$$\sigma_w = 10/\rho_w \tag{3}$$

[10] Interstitial water resistivity can be converted to salinity (S) assuming a temperature of 20°C by the following empirical relationship [*Manheim et al.*, 2004a]:

$$S = 7.042^{*}\rho_w - 1.0233 \tag{4}$$

[11] Since conductivity is a function of salinity, temperature and pressure (approximately 1 atm at the depths in question), we can use the relation $S = 7.042^{*} (10/\sigma_w)^{-1.0233}$ to determine salinity from conductivity readings. The conductivity of the pore water can then be related to σ_b through the formation factor,

$$\sigma_b = \sigma_w/F \tag{5}$$

[12] Although the pore water salinity can be estimated in this way from σ_b, it is not possible to make any quantitative statements about the flow rate of freshwater using conductivity measurements alone. However, if a correlation can be established between the two measurements as well as an understanding of the hydrologic characteristics of the site, perhaps conductivity measurements can be used to extrapolate and interpolate SGD measurements over larger areas as well as account for the separation of fresh and marine SGD.

[13] Assuming that the distribution of saline pore water is described by an advection-dispersion equation with a constant salinity (S_0) at the surface and fresh water (zero salinity) at depth, the steady state distribution is given by

$$\sigma_w = S_o e^{\omega/zD} \tag{6}$$

where

σ_w conductivity of pore water (mS cm^{-1})
S_0 salinity of the open water
ω upward velocity of water (m d^{-1})
D dispersion coefficient (m^2 d^{-1})
z depth (m)

[14] We may be able to determine what causes the site-specific disparity in the correlation between SGD and BGC. However, if the measurements made are σ_b, not salinity, and SGD is a linear flow rate measured in the overlying water column commonly reported as cm^3 cm^{-2} d^{-1}, or cm d^{-1}, not ω (ω = SGD/Φ), we must substitute relationships from 1, 2, and 3 in order to cast the equation in terms of σ_b and SGD. It must be noted here that linear flow rates are not common in coastal systems, but must be used here for the sake of the calculation, and therefore average SGD. If we take an average conductivity to some depth z_o, and use the substitutions, the equation would change to:

$$\sigma_{b(avg.)} = 1/z_o \int_o^{zo} \Phi^m \sigma_w e^{-0.977(\phi)(SGD)/zD} dz \tag{7}$$

$$\sigma_{b(avg.)} = \Phi^{-m}\sigma_w D/z_o(0.977)SGD\left[1 - e^{-(0.977(\phi)SGD/D)Zo}\right] \tag{8}$$

[15] In this case, the function is the simple solution to the advection-dispersion equation with the advective term replaced by SGD/porosity and the formation factor. As we will discuss later, the appearance of the dispersion coefficient, D, in 8, means that the measurement of the same BGC in two different settings may yield different values of SGD because the dispersion is different in the two places.

2.3. Seepage Meter Measurements

[16] Concurrently with the conductivity measurements, manual seepage meters, first described by *Lee* [1977], were deployed to directly measure flow. Such devices have been used extensively in diverse settings, primarily for their ease of use [e.g., *Burnett et al.*, 2001, 2006]. Water which enters the chamber displaces the water within the chamber into a plastic bag attached to an outlet spigot. Measuring volume and time, a flow rate can be determined. Bags are usually prefilled with 500 mL of ambient water (except when samples were collected for water quality measurements) to reduce artifacts [*Shaw and Prepas*, 1989; *Libelo and MacIntyre*, 1994] and to allow for the measurement of flow rates into the sediment (saltwater intrusion). At the study sites, chambers were arranged inshore-perpendicular and, if possible, shore-parallel transects in an attempt to observe spatial discharge patterns. Where possible, the chambers were left in place for 24 h prior to the first measurement. Samples were collected approximately every thirty minutes for periods between six and twelve hours. Near a submarine spring in Mauritius and at some locations in Ubatuba, Brazil samples were collected every 10 min as flow rates were very high and the bag filled quickly. In addition, a comparison was made with three types of automated seepage meters at Shelter Island (USA) and Ubatuba (Brazil). [*Burnett et al.*, 2006; *Stieglitz et al.*, 2007].

2.4. Study Sites

[17] Five study sites were selected by the SCOR-LOICZ working group 112 for the intercomparison of SGD measuring techniques. They were chosen for their diverse hydrogeological conditions, which are considered representative of many other coastal systems [*Burnett et al.*, 2006]. Importantly, at all sites at dominance of fresh, terrestrially derived SGD over recirculation of seawater was expected based on previous work by others or on anecdotal evidence.

At four of these sites, coincident measurements of ground conductivity and SGD flow rates through seepage meters were made. The four sites are briefly introduced here; more detailed information is given by *Burnett et al.* [2006].

2.4.1. Cockburn Sound, Australia

[18] Cockburn Sound is a large (150 km^2), sheltered, marine embayment on the western coast of Australia (Figure 1a). Much of Cockburn Sound is adjacent to a low-lying, drained sandy coastal plain [*Burnett et al.*, 2006]. The study site overlies an unconfined aquifer with high permeability which is recharged by seasonal rainfall of 0.85 m annual average of which 15–28% infiltrates the aquifer [*Smith and Nield*, 2003]. This aquifer is underlain by a layer of low permeability sediments as well as the confining Osborne formation [*Smith and Nield*, 2003]. The region is underlain by marine and continental sediments, which are overlain by a thin covering of Quaternary age deposits that act as a largely unconfined aquifer. Groundwater in the area generally flows in a westerly direction toward Cockburn Sound. There are virtually no surface streams as the soil is extremely permeable. Hydraulic conductivity in the area is large (20–1000 $m^3\ d^{-1}$) and therefore there is a relatively flat water table because less of a gradient is needed to transport water [*Smith and Nield*, 2003]. It has been hypothesized that over 70% of the nitrogen input into the bay is through groundwater discharge as much of the groundwater in the adjacent plain is characterized by a high nitrogen load [*Kendrick et al.*, 2002].

2.4.2. Shelter Island, USA

[19] Shelter Island was chosen as representative of a glacial outwash plain setting. It is underlain by a highly permeable (hydraulic conductivity >100 m d^{-1}), homogenous but anisotropic, unconsolidated aquifer representative of many coastlines located at the edge of the last glacial maximum. Shelter Island is a small island of 29.8 km^2 surface area with moderate relief of up to ~60 m [*Soren*, 1978]. The island is located in Peconic Bay to the east of Long Island (Figure 1b). Here a marine influence leads to a local annual precipitation of 117 cm, about half of which recharges the aquifer system. Surface runoff is ephemeral and insignificant [*Paulsen*, 1996]. Freshwater in the upper glacial aquifer discharges directly into the surrounding coastal water, lowering the salinity in the open coastal waters around the island [e.g., *Soren*, 1978]. Below the unconfined aquifer lie the Magothy and Lloyd Sand Member aquifers both of which contain groundwater with brackish salinities [*Soren*, 1978; *Paulsen et al.*, 2001].

[20] A narrow fringing marsh separates the bay from the coast in West Neck Bay (Figure 1b). The tide is semidiurnal and varies from 0.7 to 1.1 m. The sediment in the bay is variable, with fine to medium-grained sand located near the pier and pockets of silt found away from the pier. The bay is sheltered from the open sea, and therefore nonnautical wave action is minimal. Seepage of fresh groundwater above the water line can be observed in the intertidal zone in the form of rivulets of fresh water. Previous observations of seepage rates with a continuous seepage meter deployed close to a pier at the study site indicated seepage flow rates of up to 160 cm d^{-1}, displaying a strong correlation with tidal water level [*Paulsen et al.*, 2004]. Such flow rates are considered high for an unconfined aquifer system; at nearby sites on the same coastal-plain aquifer, SGD had been measured at rates much lower than 50 cm d^{-1} [*Bokuniewicz*, 1980].

2.4.3. Ubatuba, Brazil

[21] Ubatuba (Figure 1c) was chosen as representative of a fractured rock aquifer, likely causing highly variable SGD. Fractured rock creates preferential groundwater conduits. Granitic and magmatic mountains, over 1000 m in elevation, spill down into the bay forming the basement for groundwater flow. Groundwater flow occurs in fractures of these pre-Cambrian rocks. These rocks are overlain by highly permeable fine- to medium-grained sands. Here freshwater discharge is sufficient to reduce the salinity of local waters as seen at Shelter Island [*Oberdorfer et al.*, 2008]. Precipitation in the area is one of the highest in Brazil, averaging about 1.8 m a^{-1} [*Oliveira et al.*, 2003].

2.4.4. Flic-en-Flac Bay, Mauritius

[22] Mauritius was chosen as a site representative of volcanic island settings in which steep elevations are likely to create substantial onshore hydraulic gradients. The island of Mauritius covers 1865 km^2, and reaches elevations of up to 600 m. The average annual precipitation varies from 1.13 m on the east coast, to 0.90 m on the west coast, to 4.0 m on the central plateau [*Burnett et al.*, 2006]. The coastal zone largely comprises lagoons created by the formation of barrier coral reefs. In some places along the western and eastern coasts, groundwater discharges are clearly visible. Anecdotal evidence suggests the appearance of infrequent algal blooms (occasionally red tides), suggesting the land-derived input of nutrients into the lagoons. Much of the coast is underlain with fractured volcanic basalts leading to conduits for discharge (J. Oberdorfer, personal communication, 2005).

[23] Flic-en-Flac Bay is on the eastern coast of the island of Mauritius (Figure 1d). The embayment is partially enclosed by a fringing coral reef and is blanketed offshore with a layer (~1 m) of fine, coral sand. Much of the lagoon is covered with patchy coral. The tidal range in the bay is less than 50 cm. A well-known submarine spring is found in the area. Freshwater discharge from this submarine spring, and possibly others, is sufficient to reduce the salinity of coastal waters from oceanic salinities of 35 to salinities of 33 in the lagoon.

3. Results

[24] The results presented here represent a subset of BGC and flow data collected at the different study sites. Some of the presented data from West Neck Bay, Ubatuba, and Flic-en-Flac have been reported previously in a different context [*Stieglitz et al.*, 2007, 2008; *Bokuniewicz et al.*, 2007]. Data are presented in chronological order.

3.1. Cockburn Sound, Australia

[25] Data were collected in Cockburn Sound from 27 November to 6 December 2000. Three shore-normal transects (10 m) and one shore-parallel transect (85 m) of BGC show fresh groundwater close to the shoreline being replaced by increasingly salty groundwater with distance from the high tide mark. The transition occurs along a well-defined, shallow vertical gradient typical of unconfined aquifers [*Stieglitz*, 2005]. BGC increased from ~1 mS

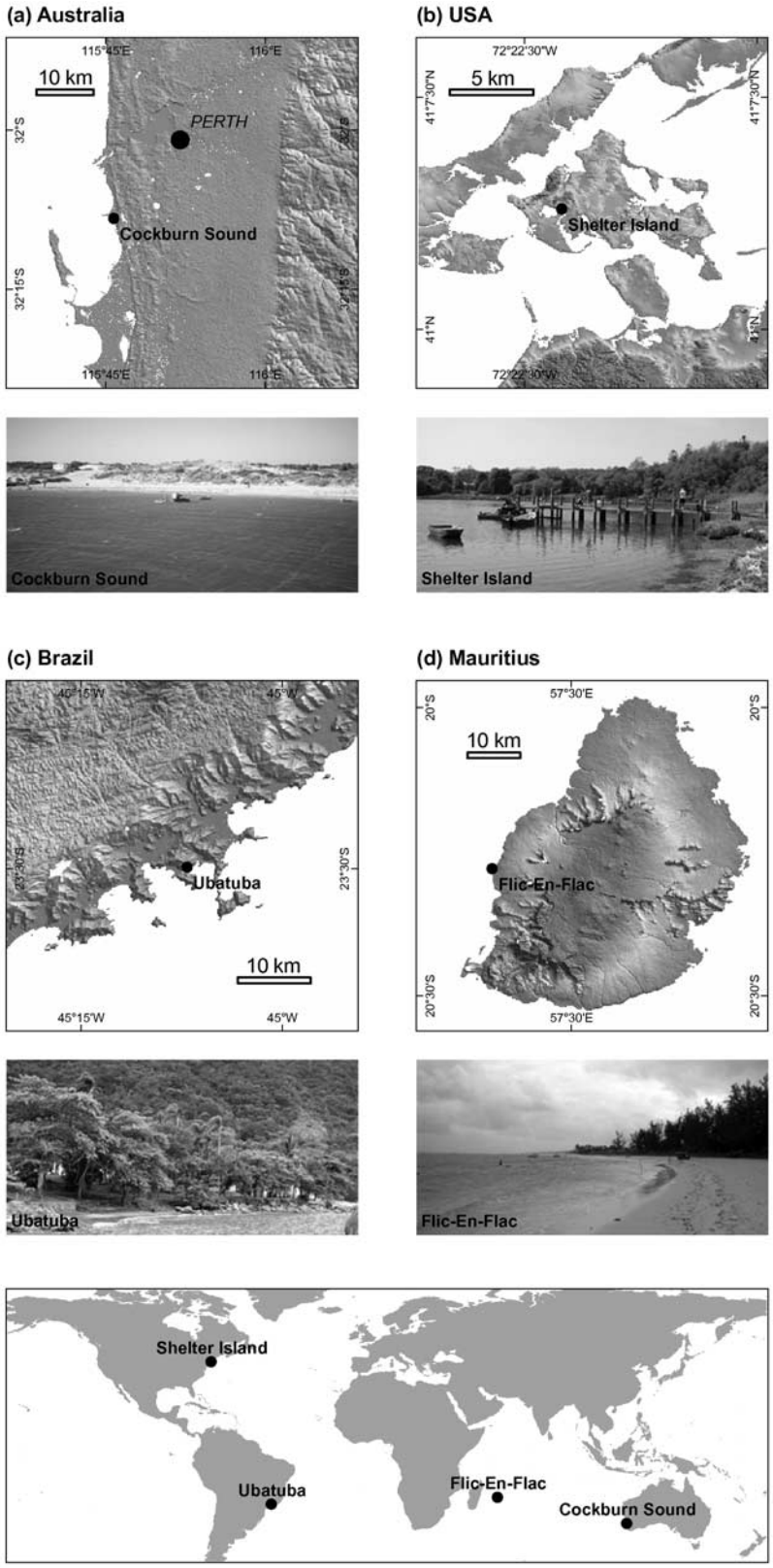

Figure 1. Location maps and photographs of the study sites (a) Cockburn Sound, Australia (b) Shelter Island, USA, (c) Ubatuba, Brazil and (d) Flic-en-Flac Bay, Mauritius. NASA SRTM data is shown to indicate the local topography.

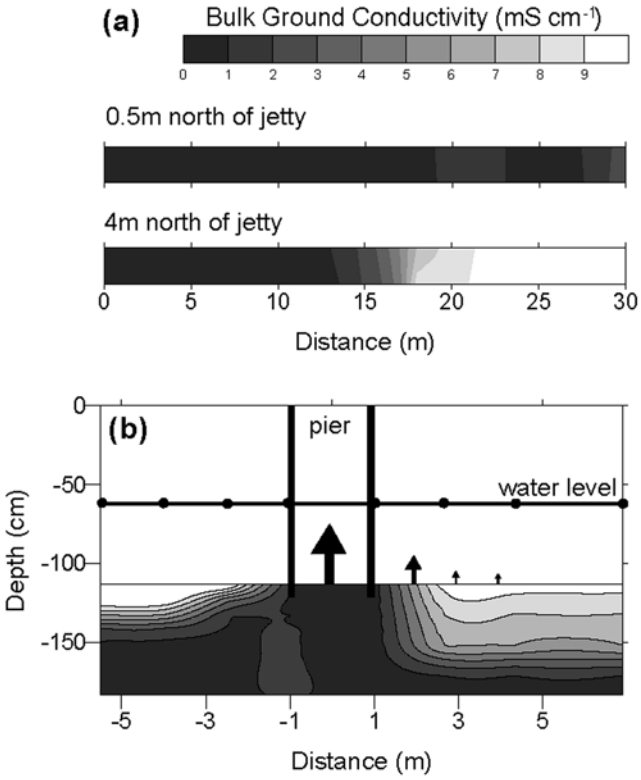

Figure 2. *Shelter Island*. (a) Bulk ground conductivity of the top 10 cm of the seabed (top) along the pier and (bottom) 4 m north of the pier at low tide (b) bulk ground conductivity along a shore-parallel transect below the pier, approximately 17 m from the mean high water level. The pilings are shown as thick lines. Dots marks the location of BGC profiles used to construct the contour plot. The length of the black arrows is approximately proportional to the average seepage flux measured at the respective location. A decrease in flow with increasing distance from the pier is apparent. Adapted from *Stieglitz et al.* [2007].

cm^{-1} near the shore to over 15 mS cm^{-1} less than 10 m from shore.

[26] Two shore-parallel transects consisting of four manual seepage meters each were deployed up to 70 m from shore. These manual seepage meters show an offshore decrease in average SGD; however, these drums were deployed offshore from the conductivity transects and therefore no direct relationship can be ascertained from these seepage meter deployments. Alongside one of the conductivity transects, an automated seepage meter was placed. Here seepage rates ranging from 4.05 to 60.88 cm d^{-1} were found, with a mean seepage rate of 32 cm d^{-1}. In addition, there was a strong inverse correlation between water elevation and SGD. This drum was deployed at a site with a medium value of BGC (6 mS cm^{-1}).

[27] Note that data from Cockburn Sound will not be used in the comparison of BGC with SGD as there is only one data point and therefore will only be used as a reference. We include this data here for completeness.

3.2. Shelter Island, USA

[28] Data were collected in Shelter Island from 17–24 May 2002. Bulk ground conductivity measurements show fresh groundwater in the sediment surrounding a pier (Figures 2a and 2b). Here, two shore-normal transects and one shore-parallel transect of BGC measurements were taken extending from the high water mark to 30 m offshore, at depths of up to two meters. In addition, a shore-normal transect of manual seepage meters measured coincident flow rates at 8, 11, and 15 m from the high tide mark. At 15 m from the high tide mark a shore-parallel transect of seepage meters (manual and automated) was placed 0, 2, 3, and 4 m from the pier.

[29] Sediment BGC values were less than 2 mS cm^{-1} directly beneath the pier, indicating pore water with very low salinity. East of the pier there was a mixing zone about 2 m wide in which BGC values increase from 2 mS cm^{-1} to 9 mS cm^{-1}. At the ambient temperature of 14°C and a seawater conductivity of 34 mS cm^{-1} (both measured directly) salinity equals 28, or using (1), 9 mS cm^{-1}. The mixing zone width (or the area in which there was a large gradient in BGC) was negatively correlated with tide and ranged from 2.5 m at high tide to 5 m at low tide. All manual seepage meter measurements showed a strong negative correlation with tide ranging from about 32.5 cm d^{-1} at low tide to less than 5 cm d^{-1} at high tide along a transect 2 m away from a pier (Figure 3). This is an expected pattern in situations where SGD is driven by onshore hydraulic gradients. However, other expected patterns, such as an exponential decrease in SGD with distance from the shoreline, were not observed [*Bokuniewicz*, 1980; *Stieglitz et al.*, 2007]. Seepage rates did, however, decrease with (alongshore) distance from the pier (Figure 3). The highest average seepage rates of 65 cm d^{-1}, with a peak flow of 190 cm d^{-1}, were recorded directly under the pier, which is consistent with previous measurements close to the pier [*O'Rourke*, 2000; *Paulsen et al.*, 2004]. Moving away from the pier, seepage rates of 25 cm d^{-1} with peak flow of 37 cm d^{-1} were recorded at 2 m distance. At 3 m and 4 m distance from the pier, the seepage rates were further reduced to 6 cm d^{-1} (peak 12 cm d^{-1}) and 2 cm d^{-1} (peak 6 cm d^{-1}) respectively [*Sholkovitz et al.*, 2003] (Figure 3 and Table 1).

[30] The salinity of water collected by the seepage meters increased with distance from the pier. When the devices were flushed, salinity averaged 10, 19, and 27 in the chambers located 2, 3, and 4 m from the pier respectively.

[31] SGD decreased exponentially with increasing BGC, and with distance from the pier (Figure 3 and Table 1). At sites of high BGC, the discharge was low but not zero, suggesting a comparatively small volume of discharge of recirculated seawater. This water is likely driven into the sediment by tidal pumping, due to the presence of a reasonable tidal range (> 1 m). Both the magnitude of the SGD and the width of the "low BGC" zone seem to be related to the tidal elevation. During ebb tide, the SGD in each of the devices increased by a factor of 2–4 while the "low BGC" zone widened by a factor of 2. This is likely to be due to a greater net water table hydraulic gradient present at low tide. BGC at this site is averaged over time, as the BGC in certain locations changes with changing tidal elevation. Therefore the relationship discussed here only considers the average BGC value. Directly under the pier, for instance, the flow rate is negative at high tide, while BGC remains low. The reason for this may be that SGD

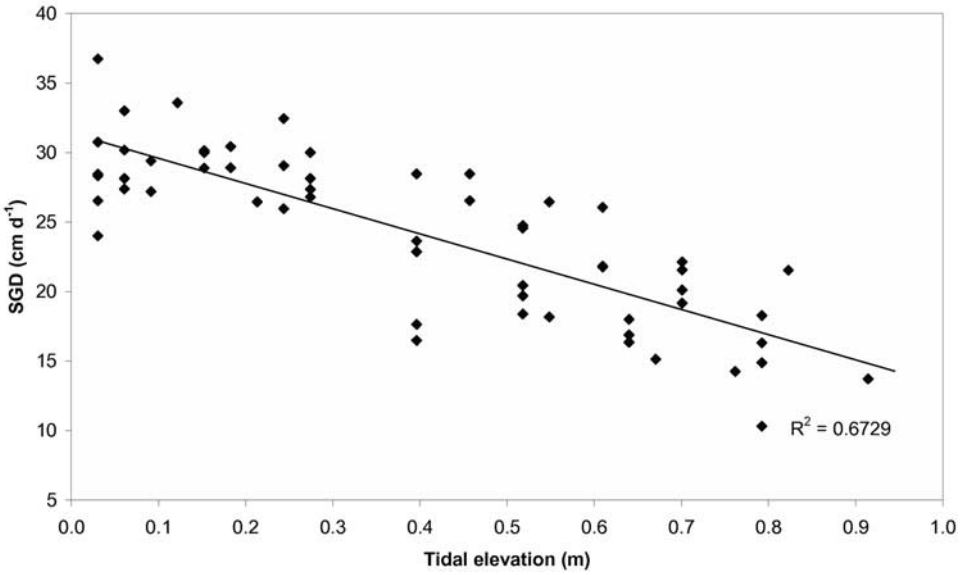

Figure 3. *Shelter Island*. Seepage rates versus tidal elevation measured along a transect parallel to the pier, (locations of the seepage meters are indicated in Figure 1).

does not remain negative long enough for sufficient salt penetration into the sediments directly under the pier, although it does on the fringe of the ''low BGC'' zone.

3.3. Ubatuba, Brazil

[32] Data were collected in Brazil on 16–22 November 2003. BGC profile data were collected along a shore-normal transect in Flamengo Bay (Figure 4). In Figure 4, the slope of the beach and the water level at the time of recording are included.

[33] Manual seepage meters were placed along both shore-parallel and shore-normal transects. The shore-parallel transect consisted of three seepage meters at the low tide line. Seepage meters in the shore-normal transect were located at distances of 5, 10, 18, 32, and 44 m from the low-tide shoreline at (water) depths of 0.33, 0.71, 1.07, 1.46, and 1.65 m respectively. Though the highest discharge (268 cm d^{-1}) was measured close to shore, SGD in the shore-parallel transect was variable over small distances. Indeed, discharge decreased with distance from shore, although the 5th and 6th locations also displayed significant flow rates [*Bokuniewicz et al.*, 2004]. The lowest salinity (~20) was measured in the seepage meter with the highest flow rate (Table 2).

[34] As on Shelter Island, measured flow rates were highly dependent on location. Salinity in the chambers did show a correlation with flow rates, though the range of salinity (20–30) was not nearly as great as in Shelter Island (6–28). Conductivity measurements showed that a layer separating high from low BGC sediments was present about 50 cm beneath the surface, (Figure 4). Concurrent profiles of pore water salinity and BGC at Ubatuba presented by *Stieglitz et al.* [2008] demonstrate a close relationship of pore water salinity with BGC at all depths of the transect. Where the low conductivity fraction extends toward the surface, higher flow rates are measured within the chambers. As the location of advection of fresh water in this site is likely to be controlled by the spacing of fractures, the

Table 1. Colocated Average SGD Flux and BGC Data From the Four Study Sites[a]

Site	Seepage Meter	AVG. SGD, cm d^{-1}	AVG BGC, mS cm^{-1}
Cockburn sound	AUTO1	32	6.0
Shelter Island	MSRC1	22	4.2
Shelter Island	MSRC2	24	4.1
Shelter Island	MSRC3	25	4.0
Shelter Island	WHOI	6	9.0
Shelter Island	USFM	65	0.5
Shelter Island	SFWMD	2	11.0
Ubatuba Bay	S1	40	10.0
Ubatuba Bay	S2	10	7.0
Ubatuba Bay	S8	70	15.0
Flic-en-Flac	M1	216	0.5
Flic-en-Flac	M2	18	15.0
Flic-en-Flac	M3	108	9.0
Flic-en-Flac	M4	21	14.5
Flic-en-Flac	M5	14	0.5
Flic-en-Flac	M6	301	15.5
Flic-en-Flac	M7	11	14.5
Flic-en-Flac	M8	20	15.0
Flic-en-Flac	M9	8	15.0
Flic-en-Flac	M10	6	15.0
Flic-en-Flac	M11	8	15.5
Flic-en-Flac	M12	3	15.0
Flic-en-Flac	M13	166	5.0
Flic-en-Flac	M14	124	8.0
Flic-en-Flac	M15	362	0.5
Flic-en-Flac	M16	5	15.5
Flic-en-Flac	M17	6	15.5
Flic-en-Flac	M18	10	15.0
Flic-en-Flac	M19	32	14.0
Flic-en-Flac	M20	4	15.0
Flic-en-Flac	M21	16	15.0
Flic-en-Flac	M22	9	15.0
Flic-en-Flac	M23	8	15.5
Flic-en-Flac	M24	4	15.5
Flic-en-Flac	M25	3	15.5
Flic-en-Flac	M26	17	15.5

[a]These data are plotted in Figure 7.

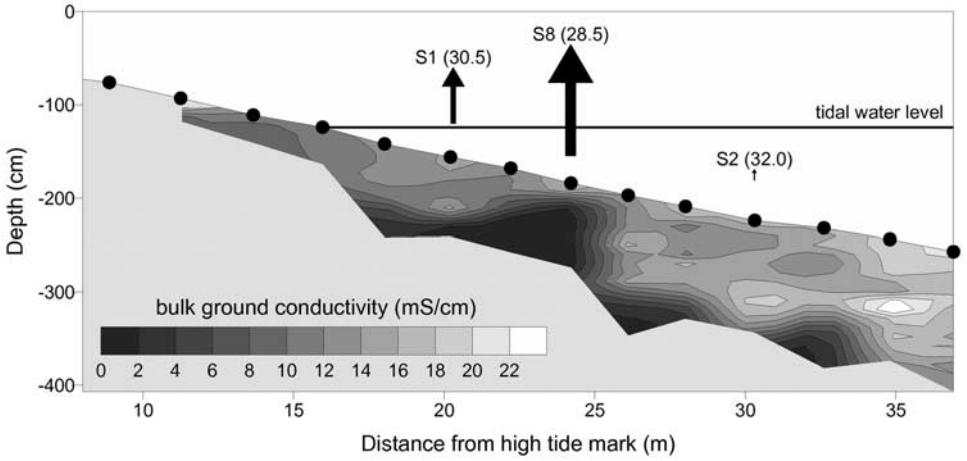

Figure 4. *Ubatuba*. Representative ground conductivity transect. At each of the stations along the transect (indicated by solid dots on the sediment surface), a profile of ground conductivity was recorded, and data was subsequently contoured. The tidal water level at time of recording each transect is indicated. The arrows at stations 10, 12, and 15 mark the locations of the manual seepage meters S1, S8, and S2 respectively. The length of the arrows is proportional to the average flux of SGD into each of these seepage meters, and the average salinity of the SGD is provided in brackets. Figure adapted from *Stieglitz et al.* [2008].

pool of lower conductivity water was probably affected by the presence of one of these fractures.

3.4. Flic-en-Flac Bay, Mauritius

[35] Data were collected on 18–25 March 2005. BGC was measured in a 20,000 m^2 grid surrounding a known point of freshwater discharge. Here measurements were taken every 5 m in 100-m-long offshore transects every 10 m along the beach. At each location, BGC was measured at 5 depths up to a maximum of 2 m in the sediment. Between locations in which there was a comparatively large gradient in BGC, additional profiles were recorded to achieve higher resolution. Maximum BGC was about 14 mS cm^{-1} corresponding to average surface water salinity in the area (~33). BGC in the sediment directly next to the spring was 0–1 mS cm^{-1}. The influence of the spring was widespread, as low BGC values were found within a 25 m radius of the spring. Outside of this radius, we measured a sharp transition zone (5 m) between low (<3 mS cm^{-1}) and high (>10 mS cm^{-1}) BGC (Figure 5).

[36] Nine chambers were placed at a total of 24 locations. These seepage devices were deployed in three shore-normal transects (one adjacent to the spring, one in a cove 1000 m north of the spring, and one about 500 m south of the spring), as well as in a 1500 m shore-parallel transect, corresponding to areas of low BGC as were measured on the first day of the experiment.

[37] The first shore-normal transect consisted of five devices located adjacent to the known submarine spring. The shoreward device (M1) was placed at a water depth of 50 cm. The other four devices (M3, M6, M5, and M4) were placed at distances of 20, 50, 80, and 150 m from the low-tide shoreline. The respective water depths at low tide were 1.6, 1.9, 1.4, and 1.6 m. The tops of the devices were between 0.04 and 0.1 m above the seafloor. Measurements were taken at this transect over a period of 72 h. The other two shore-normal transects will not be discussed in this paper.

[38] The shore-parallel transect consisted of measurements taken at various times from devices deployed within 15 m of the low tide line. This transect consisted of 18 devices which were in place for a period of 10 h to 5 d. Not all measurements along this transect were made simultaneously; however, at least six devices along this transect measured SGD throughout the sampling period.

[39] The measured seepage rates were variable over the entire study area, ranging from negative seepage (i.e., flow of lagoon water into the sediment) to SGD of >490 cm d^{-1}. Devices placed near the spring recorded high rates while devices placed away from the spring recorded consistently lower flow rates.

[40] The presence of the spring precluded the observation of an offshore decrease in SGD, and was evident in the alongshore transect. All of the devices in the alongshore transect were deployed in permeable, visually homogeneous carbonate sands. SGD was 216 cm d^{-1} south and shoreward of the spring. At the same distance north of the spring, SGD was found to occur at a value of between 5 and 15 cm d^{-1}, more typical of the rest of the Flic-en-Flac Lagoon.

[41] Only in the vicinity of the spring did the benthic chambers collect water with a significantly different salinity than the ambient lagoon water. Here waters with a salinity as low as 5 were collected by the benthic chambers. In addition, a linear inverse correlation was seen between salinity and SGD rates.

Table 2. Total SGD Flux and Freshwater Fraction as Calculated From Equations (8), (9), and (10)

Site	Total SGD, 10^3 m^3 d^{-1} km^{-1}	Freshwater Fraction	Fresh SGD, 10^3 m^3 d^{-1} km^{-1}
Cockburn sound	2.91	41%	1.20
Shelter Island	1.59	24%	0.38
Ubatuba	7.16	29%	2.08
Flic-en-Flac	245.00	63%	154.00

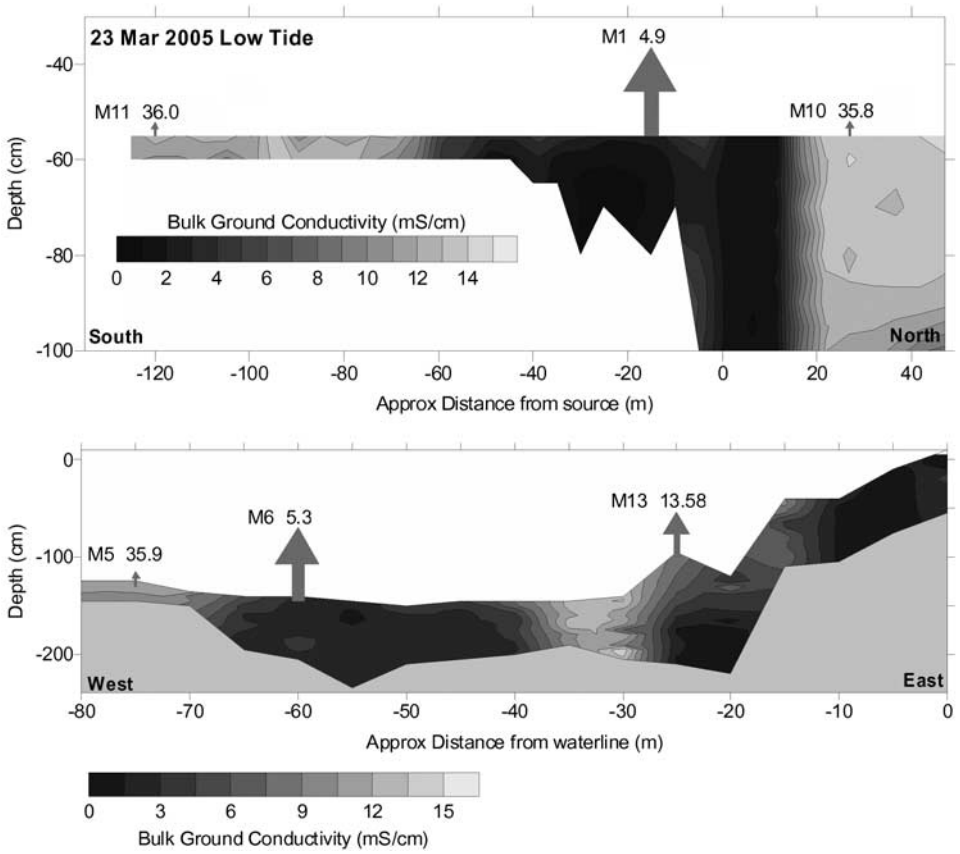

Figure 5. *Flic-en-Flac*. (a) Alongshore and (b) shore-normal transects of conductivity in the vicinity of the freshwater spring in Flic-en-Flac bay. The arrows represent relative SGD rates as measured in benthic chambers, and the average salinity of the SGD is denoted next to each instrument number. Similar to Figures 2 and 4, the interpolated transects have an irregular bottom boundary as contours we're only drawn to the depth of the measurement. Sediment characteristics (i.e., location of buried coral) precluded the penetration to the same depth everywhere in the transect.

[42] Below a flow rate of 200 cm d^{-1}, a negative, linear correlation between BGC and SGD in the chambers was observed. At flow rates greater than 200 cm d^{-1}, SGD had the same salinity as the water coming directly out of the spring. Average flow rates increased to close to 400 cm d^{-1} at this site and therefore it will be difficult to distinguish flows above 200 cm d^{-1} with BGC measurements alone. Salinities inside the chambers were inversely correlated with BGC measurements as well. At this site the flow rates, though variable, showed no correlation with tide. This suggests that flow was driven primarily by the submarine spring. Of the 24 seepage meters which recorded ambient salinity and high BGC, the average flow rate was 10 cm d^{-1} with a maximum rate of 30 cm d^{-1} (Table 1). Note that the values seemed to depend on the beach slope, with the higher SGD occurring near steeper gradients. The fairly large recirculated component of SGD at this site suggests enhanced mixing processes within the upper few centimeters of sediment.

4. Discussion

4.1. Interpretation of BGC Results

[43] In these studies, BGC is clearly site-dependent with a sharp interface between high and low BGC at the sediment surface at certain sites, while at other sites there is a nonuniform BGC distribution. In Cockburn Sound, BGC distribution was likely controlled by the discharge of fresh groundwater close to the shoreline as BGC increased rapidly from less than 1 mS cm^{-1} (fresh pore water) to more than 15 mS cm^{-1} (saltwater) within 10 m of the shore. In Shelter Island, BGC was high except along the shoreline as well as the immediate vicinity of the pier. In both of these cases, the transition zone was sharp, the gradient being between <1 mS cm^{-1} and 10 mS cm^{-1}. It is likely, that at this site BGC was controlled by processes involving the emplacement of the pier. In Ubatuba Bay, BGC is hypothesized to be dependent on fractures in the basaltic rock below the sandy sediment [*Stieglitz et al.*, 2008]. Once again we found sharp gradients in the BGC from less than 1 mS cm^{-1} to greater 14 mS cm^{-1}. In Mauritius, BGC was clearly controlled by the location of the freshwater spring as abrupt transitions were found in every direction about 10–15 m from the center of the visible spring. In addition, along the beach there was a small zone of low BGC, where higher flow rates were found.

4.2. Interpretation of Seepage Meter Results

[44] SGD as recorded by seepage meters similarly depended on location in the area and, in general, corre-

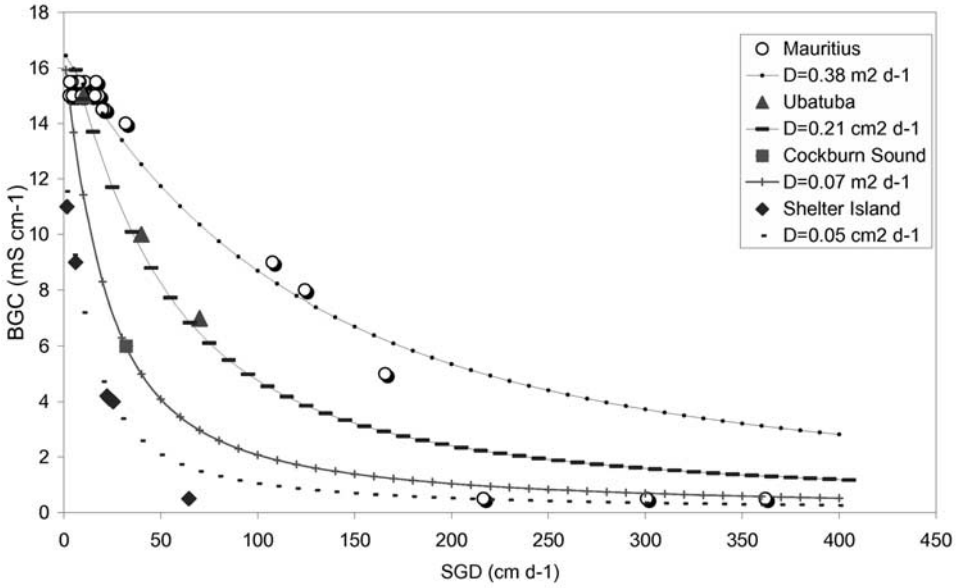

Figure 6. The relationship BGC and SGD at the four sites. Data from Cockburn Sound, Shelter Island, Ubatuba, and Mauritius are denoted by squares, diamonds, triangles, and hollow circles respectively. The curves represent the relationship in equation 8 at different values of the dispersion coefficient D.

sponded very well with zones of low BGC. However, this negative correlation between BGC and SGD was site-dependent, and seemed to be based on several factors which will be discussed in the next section (Figure 6). In Cockburn Sound, high rates of seepage were located in the vicinity of the shoreline, and therefore characteristic of a coastal zone site in which SGD is driven by the onshore hydraulic gradient, which follows basic hydrogeological theory [*Hubbert*, 1940; *Bokuniewicz*, 1980]. Meanwhile in Shelter Island, average seepage decreased exponentially from 65 to 2 cm d^{-1} within a distance of 4 m from the pier. In Ubatuba, discharge was irregular, with rates varying from 8 to 280 cm d^{-1}, most likely caused by fractures in the basaltic basement. Discharge of great magnitude was found near and above the spring in Mauritius (>490 cm d^{-1}). According to local anecdotal knowledge, a large lava tube may serve as a high-flow conduit or ''underground river''. Discharge was relatively low elsewhere at this site, but not insignificant, suggesting that in the absence of freshwater discharge recirculated seawater is discharging, perhaps driven into the sediment by bioirrigation, tidal pumping or wave set-up.

4.3. Interpretation of Relationship Between BGC and SGD

[45] A family of curves is plotted in Figure 6 showing BGC as a function of SGD (Table 1) from (7) or various values of the dispersion coefficient, D, ranging from 0.05 to 0.38 m^2 d^{-1} assuming a average depth (z_0) of 1 m, a porosity (Φ) of 0.5 and an exponent (m) of 1.2, together with data from the different study sites.

[46] At each of the sites, a direct relationship between conductivity and SGD measured from seepage meters was observed. Tidally averaged SGD versus BGC (Figure 6) shows variations in the curves among the 4 sites. While at Mauritius the linear correlation makes it fairly easy to approximate SGD from BGC, at Shelter Island the relationship is exponential and, therefore, more complex. The difference in curves between sites is most likely due to variation in the dispersion of salt downward and the formation factor of the sediments. In this interpretation, Shelter Island has the lowest vertical dispersion. The relationship between BGC and SGD at this site is averaged over time. Directly under the pier, the flow rate is negative at high tide, while the BGC remains low. The most likely reason is that SGD does not remain negative long enough for significant salt penetration into the sediments directly under the pier, while it does on the fringe of the ''low BGC'' zone (seepage rates show that the salt would penetrate less than 2 cm into the sediment before the flow changed direction, expelling the salt). Also, the flow rates do not remain negative for more than a half hour per tidal cycle, therefore it is possible that the BGC measurements missed this period of salt water intrusion. Dispersion at Ubatuba is higher than at Shelter Island, while dispersion at Mauritius is highest for low values of SGD and lower for higher values of SGD. The values of the vertical dispersion of salt is critical, because BGC can be a proxy of how far salt can disperse downward into the sediment against an upward advection of (fresh) groundwater. Molecular diffusion of salt through the pore water is insufficient to move salt downward against even a small upward advection, so other, more efficient mixing processes must be operative.

[47] Here we will consider dispersion to include any process other than advection which causes the movement of solutes. The mechanism for the vertical dispersion of salt against the upward advection (i.e., SGD) likely varies between places due to local hydrogeological characteristics. For example the type of sediment may prevent in-mixing of salt water therefore causing the BGC to freshen at a much lower upward advection rate. At Shelter Island, the sediment ranged from fine sand to silt, at Flic-en-Flac the

sediment was fine- to medium-grained carbonate sands, and at Ubatuba Bay, the area was underlain by coarse sands. Though no permeability tests were carried out at these sites, it is reasonable to assume that salt water penetrates into the sediment with greater ease at Ubatuba and Flic-en-Flac as sand has a higher permeability than silt. Other characteristics which are likely to influence in-mixing of saline water include the salinity of the ambient water. Higher salinity waters will have a large density difference as compared to fresh pore water and therefore penetrate further into the sediment through salt-fingering [*Seplow*, 1991; *Bokuniewicz et al.*, 2004]. At Mauritius the surface salinity ranged between 30 and 35 (46–54 mS cm^{-1}) while at Shelter Island the surface salinity was 26–28 (31–34 mS cm^{-1}). *Bokuniewicz et al.* [2004] suggested that dispersion due to density mixing could be on the order of 0.007–0.03 m^2 d^{-1}. A further possibility is saline water penetration due to wave setup. As waves approach a beach they create a sloping water table, with larger waves creating a greater gradient. There are virtually no waves at Shelter Island, while at Mauritius and Ubatuba Bay, even though reefs protects the beach, sometimes comparatively high waves (>1 m) come ashore. Though individual waves should not change set up long enough to make a difference, a constant occurrence of waves may be important. Note that *Colbert and Hammond* [2008] demonstrate that individual waves can impact hydraulic gradients which may affect the SGD and therefore the correlation in some cases. Tidal pumping [*Ataie-Ashtiani et al.*, 1999; *Taniguchi et al.*, 2005] has been known to lead to an intrusion of salt water. An inflow of water at velocities between 0.0084 and 0.042 m d^{-1} has been suggested [*Ataie-Ashtiani et al.*, 1999]. Though the tidal range is greater at Shelter Island than at Mauritius, it seems that the other characteristics dominate the ability to disperse salt into the sediment.

[48] Bioirrigation may aid in the in-mixing of salt water to the sediment; *Jaeger et al.* [2005] suggest a mixing coefficient of 0.001 m^2 d^{-1} due to bioturbation alone, while *Martin et al.* [2006] suggested a linear velocity of 0.05 m d^{-1}. In the case of the Indian River Lagoon in Florida [*Martin et al.*, 2006], bioirrigation was considered to be the major source of seawater mixing into the sediment. It is likely that bioirrigation rates vary between sites, as this process is dependent both on the type of sediment as well as the type and prevalence of organisms that live within them [*Schlueter et al.*, 2000]. For example, the rate of bioirrigation of a single burrow differs from 0.007 m^2 d^{-1} for shrimp (e.g., *Calianassa sp*.) to 0.003 m^2 d^{-1} for worms (e.g., *Arenicola*) [*Martin et al.*, 2006].

4.4. Extrapolation of SGD Values From BGC Measurements

[49] As previously noted, an important limitation of point measurements of SGD flux with seepage meters is that such measurements will only be a good representation of the discharge where SGD is homogenous, which is often not to be the case, as the examples presented here illustrate. Commonly, total SGD flux from an area (as opposed to a single point, i.e., a seepage meter) is reported in the form of discharge volume per time unit per shoreline unit, whereby the spatial variability of discharge is not taken into account. We suggest that comparing point SGD measurements with BGC as presented here, thereby accounting for spatial variability, will result in an improved estimation of SGD within the study area.

[50] Adjusting the value of D (the dispersion coefficient) in equation (8), we are able to reproduce the relationship between SGD and BGC for each site (Figure 6). The correlation at Shelter Island corresponds to a dispersion coefficient of 0.05 m^2 d^{-1}, while at Mauritius it is closer to 0.38 m^2 d^{-1}. Thus dispersion is nearly an order of magnitude larger within the sediment at the Mauritius site, although above an apparent threshold of 150 cm d^{-1}, the mixing seems to more closely match the correlation observed at Shelter Island. Processes such as bioturbation, tidal pumping, wave set-up, and density-driven salt fingers have been previously discussed, in addition to differences among the sediment porosity and permeability [*Ataie-Ashtiani et al.*, 1999; *Li et al.*, 1999; *Taniguchi et al.*, 2005; *Jaeger et al.*, 2005]. The dispersion coefficient is likely to be a function of all of these characteristics. It is reasonable to assume that this suite of factors varies between sites, which explains the observed differences in effective dispersion value between sites.

[51] Based upon the correlation between BGC and SGD as well as the area covered by BGC measurements we can approximate total discharge per meter of shoreline into the study areas, whereby we effectively use the BGC as weight in a weighted-average calculation of SGD flux. Using the Cockburn Sound BGC data to interpolate SGD throughout the study site (3200 m^2), and assuming high magnitude SGD occurs only in the vicinity of the shoreline [*Burnett et al.*, 2006], the total discharge into Cockburn Sound is 2.91×10^3 m^3 d^{-1} km^{-1} of shoreline. This number agrees very well with SGD calculated using both radon (2.0 to 2.7×10^3 m^3 d^{-1} km^{-1}) and radium (3.15×10^3 m^3 d^{-1} km^{-1}) as tracers [*Burnett et al.*, 2006]. For Shelter Island, interpolating the BGC data throughout the study site (3000 m^2) and, assuming the high discharge only occurs at the immediate shoreline and in the vicinity of the pier pilings, the total discharge into West Neck Bay is 1.59×10^3 m^3 d^{-1} km^{-1} of shoreline (Table 2). This number agrees well with modeling estimates ($0.3–1.4 \times 10^3$ m^3 d^{-1} km^{-1}) but is less than that calculated using radium and radon ($16–26 \times 10^3$ m^3 d^{-1} km^{-1} of shoreline). We suggest that this is likely due to the radon and radium tracers having been collected in the vicinity of the pier and the then unknown effect of the pier not having been taken into account in the flux calculations [*Burnett et al.*, 2006; *Stieglitz et al.*, 2007]. In Brazil, the interpolation of BGC data throughout the

Figure 7. Contour maps of SGD at Shelter Island (top), Ubatuba (middle), and Flic-en-Flac (bottom) respectively, showing nonuniform SGD distribution at all sites. The SGD distribution is interpolated from BGC and seepage meter data using the model shown in Figure 6. The SGD contours are calculated from surface BGC data collected in a grid with a spacing of approximately 5 m in both directions, except in areas where strong gradients were found where grid spacing was reduced to approximately 2 m in order to capture the gradients more accurately.

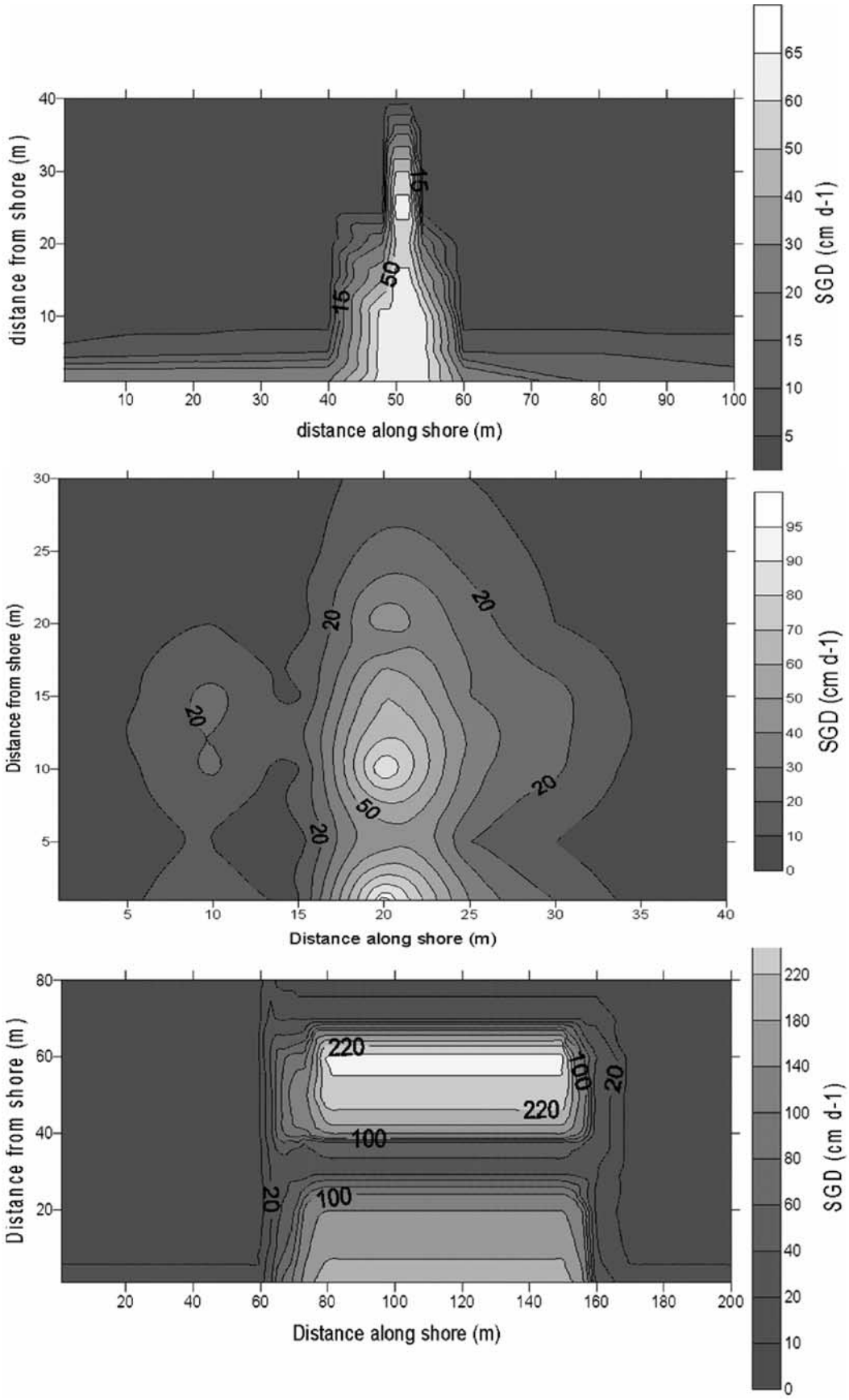
distance from shore (m)
distance along shore (m)
SGD (cm d-1)
Distance from shore (m)
Distance along shore (m)
SGD (cm d-1)
Distance from shore (m)
Distance along shore (m)
SGD (cm d-1)

Figure 7

study area (1200 m^2) yields a total discharge into Ubatuba Bay of 7.16×10^3 m^3 d^{-1} km^{-1} of shoreline. All methods (seepage meters, tracers, and models) at Brazil showed large spatial variability in the SGD estimates. The results presented here are well within the range of those previously reported [*Burnett et al.*, 2006]. In Mauritius, the BGC data throughout the study site (12,000 m^2) yields a total discharge into Flic-en-Flac bay of 2.45×10^5 m^3 d^{-1} km^{-1} of shoreline. These numbers are higher than those reported using radon as a tracer (1.3×10^4 m^3 d^{-1} km^{-1}) [*Burnett et al.*, 2006], although this is expected due to the bias of point measurements made near the spring (Figure 7).

[52] SGD measurements across a study site can be improved by taking BGC distribution into account, provided the maximum and minimum average SGD values are known and the relationship between SGD and BGC can be established (i.e., the shape and intercepts of the curve can be derived). Both BGC and the relationship between BGC and SGD are site dependent. Therefore the investigation of BGC at a site can aid the understanding of site characteristics influencing SGD, most importantly the dispersion properties of the sediment.

[53] Considering the data from Mauritius, for example, a BGC measurement corresponding to a salinity of 15 would be proportional to a discharge of 100 cm d^{-1}, while at Shelter Island this same BGC measurement would suggest a discharge of 30 cm d^{-1}. Our findings suggest that the difference between these two sites are at least in part due to site-specific sediment properties.

4.5. Determination of the Freshwater Fraction of Discharge

[54] Recirculated seawater is an important component of SGD in many cases. If the SGD consists to 100% of seawater, there will be no gradient in pore water salinity, or BGC, from which to deduce SGD as described above. A detectable pore water salinity gradient, whether measured directly or through BGC, can be interpreted in terms of a dispersion coefficient. The correlation between BGC and SGD data can also be used to determine the relative inputs of fresh and recirculated seawater by the following calculation

$$q_s = \sigma_b/(\sigma_s - \sigma_f)*Q \quad (9)$$

and

$$q_f = Q - q_s \quad (10)$$

where

q_s discharge of saltwater in cm d^{-1}
q_f discharge of freshwater in cm d^{-1}
Q total discharge in cm d^{-1}
σ_b measured BGC in mS cm^{-1}
σ_s max BGC of saline water in mS cm^{-1}
σ_f min BGC of water in mS cm^{-1}

[55] This relationship assumes a linear correlation between BGC and SGD and does not consider how the process of mixing in the subterranean estuary would affect the values. It is therefore considered an approximation only.

[56] Using the Mauritius example, at a σ_b of 9 mS cm^{-1} corresponding to a Q of 110 cm d^{-1} (Figure 6) with a σ_s of 15 mS cm^{-1} and σ_f of 0 mS cm^{-1}, the fresh water and (recirculated) seawater discharge can be calculated to be 44 cm d^{-1} and 66 cm d^{-1} respectively.

[57] Using the correlation between BGC and SGD shown in Figure 6, we can extrapolate BGC measurements from the entire study site to determine the freshwater fraction of SGD in each of the sites. In other words, using the discharge estimates from the previous section with equations (9) and (10), we can determine the freshwater fraction of the SGD into the four study areas and therefore the total freshwater discharge. The freshwater fraction of SGD in Cockburn Sound was 41%, yielding a total fresh discharge of 1.20×10^3 m^3 d^{-1} km^{-1} shoreline. In Shelter Island, the freshwater fraction was 24% of the total discharge or 0.38×10^3 m^3 d^{-1} km^{-1}. In Ubatuba, the freshwater fraction is 29% of the total discharge or 2.08×10^3 m^3 d^{-1} km^{-1}, consistent with the estimate by *Cable and Martin* [2007] who derive a highly variable freshwater fraction ranging from 4 to 87% of the total discharge at the same site. At Flic-en-Flac, the freshwater fraction is estimated to be 63% of the total discharge or 1.54×10^5 m^3 d^{-1} km^{-1} (Table 2).

5. Conclusion

[58] A strong relationship between SGD and BGC can be expected at sites where freshwater discharge is important, as is demonstrated here in a variety of settings. Point SGD flux measurements can be extrapolated/interpolated to larger areas from BGC data by taking the BGC distribution into account in the extrapolation/interpolation. We suggest that with this method, an improved SGD estimate can be derived from the point measurements. Using the correlation between BGC and SGD measurements with seepage meters, both the total discharge and freshwater fraction of SGD have been estimated in four diverse hydrogeological settings. The results agree well with previously reported values. Future studies of SGD flux can benefit from the incorporation of BGC surveys in order to better understand the processes occurring at specific study sites. A further improvement can be achieved by validating the BGC measurements with periodically collected simultaneous pore water salinity profiles and comparing the two parameters.

[59] **Acknowledgments.** The intercomparison experiments were carried out by an international working group partially funded by SCOR (Scientific Committee on Oceanic Research), LOICZ (Land-Ocean Interactions in the Coastal Zone), IOC (Intergovernmental Oceanographic Commission) and the IAEA (International Atomic Energy Agency). Too many colleagues to be named here helped with organization of the experiments and collection of data – in lieu, we thank the working group coordinators B. Burnett, E. Kontar and P. Povinec. This manuscript has benefited from the thoughtful suggestions of the James Kirby and two anonymous reviewers.

References

Ataie-Ashtiani, B., R. E. Volker, and D. A. Lockington (1999), Tidal effects on sea water intrusion in unconfined aquifers, *J. Hydrol.*, *216*, 17–31.

Beck, A. J., J. P. Rapaglia, J. K. Cochran, and H. B. Bokuniewicz (2007), Radium mass-balance in Jamaica Bay, NY: Evidence for a substantial flux of submarine groundwater, *Mar. Chem.*, *106*, 419–441.

Bokuniewicz, H. (1980), Groundwater seepage into Great South Bay, New York, *Estuarine Coastal Shelf Sci.*, *10*(4), 437–444.

Bokuniewicz, H., R. Buddemeier, B. Maxwell, and C. Smith (2003), The typological approach to submarine groundwater discharge (SGD), *Biogeochemistry*, *66*(1–2), 145–158.

Bokuniewicz, H. J., E. Kontar, M. Rodriguez, and P. A. Klein (2004), Submarine groundwater discharge patterns through a fractured rock aquifer: A case study in the Ubatuba coastal area, Brazil, *Rev. Asoc. Argent. Sedimentol.*, *11*, 9–16.

Bokuniewicz, H., J. Rapaglia, and A. Beck (2007), Submarine groundwater discharge from a volcanic island: A case study of Mauritius Island, *Int. J. Oceans Oceanogr.*, in press.

Breier, J. A., C. F. Breier, and H. N. Edmonds (2005), Detecting submarine groundwater discharge with synoptic surveys of sediment resistivity, radium, and salinity, *Geophys. Res. Lett.*, *32*, L23612, doi:10.1029/2005GL024639.

Burnett, W. C., and H. Dulaiova (2006), Radon as a tracer of submarine groundwater discharge into a boat basin in Donnalucata, Sicily, *Cont. Shelf Res.*, *26*, 862–873.

Burnett, W. C., M. Taniguchi, and J. Oberdorfer (2001), Measurement and significance of the direct discharge of groundwater into the coastal zone, *J. Sea Res.*, *46*(2), 109–116.

Burnett, W. C., et al. (2006), Quantifying submarine groundwater discharge in the coastal zone via multiple methods, *Sci. Total Environ.*, *367*(2–3), 498–543.

Cable, J. E., and J. B. Martin (2007), In situ evaluation of nearshore marine and fresh pore water transport into Flamengo Bay, *Estuarine Coastal Shelf Sci.*, *76*, 473–483.

Colbert, S. L., and D. E. Hammond (2008), Shoreline and seafloor fluxes of water and short-lived Ra isotopes to surface water of San Pedro, Ca, *Mar. Chem.*, *108*, 1–17.

Crusius, J., D. Koopmans, J. F. Brattons, M. A. Charette, K. Kroeger, P. Henderson, L. Ryckman, K. Halloran, and J. A. Colman (2005), Submarine groundwater discharge to a small estuary estimated from radon and salinity measurements and a box model, *Biogeosciences*, *2*, 141–175.

Hubbert, M. K. (1940), The theory of ground water motion, *J. Geol.*, *48*(8), 785–944.

Jaeger, J., K. Hartl, J. Cable, and J. B. Martin (2005), Evaluating the role of bioirrigation in submarine groundwater discharge (abstract), *Annual Meeting*, *Geol. Soc. Am.*, Salt Lake City, 16–19 October.

Johannes, R. E. (1980), The ecological significance of the submarine discharge of groundwater, *Mar. Ecol. Prog. Ser.*, *3*, 365–373.

Kaleris, V. (2005), Submarine groundwater discharge: Effects on hydrogeology and of near shore surface water bodies, *J. Hydrol.*, *325*, 96–117.

Kendrick, G. A., M. J. Aylward, B. J. Hegge, M. L. Cambridge, K. Hillman, A. Wyllie, and D. A. Lord (2002), Changes in seagrass coverage in Cockburn Sound, Western Australia between 1967 and 1999, *Aquat. Bot.*, *73*, 75–87.

Kermabon, A., C. Gehin, and P. Blavier (1969), A deep-sea electrical resistivity probe for measuring porosity and density of unconsolidated sediments, *Geophysics*, *34*(4), 554–571.

Lee, D. R. (1977), A device for measuring seepage flux in lakes and estuaries, *Limnol. Oceanogr.*, *22*(1), 140–147.

Lee, D. R. (1985), Method for locating sediment anomalies in lakebeds that can be caused by groundwater flow, *J. Hydrol.*, *79*, 187–193.

Li, L., D. A. Barry, F. Stagnitti, and J. Y. Parlange (1999), Submarine groundwater discharge and associated chemical input to a coastal sea, *Water Resour. Res.*, *35*(11), 3253–3259.

Libelo, E. L., and W. G. Macintyre (1994), Effects of surface-water movement on seepage-meter measurements of flow through the sediment water interface, *Appl. Hydrol.*, *4*(94), 49–54.

Maerki, M., B. Wehrli, C. Dinkel, and B. Muller (2004), The influence of tortuosity on molecular diffusion in freshwater sediments of high porosity, *Geochim. Cosmochim. Acta*, *68*(7), 1519–1528.

Manheim, F. T., D. E. Krantz, D. D. Snyder, and B. Sturgis (2004a), Streamer resistivity surveys in Delmarva coastal bays, paper presented at *Proc. Symp. Applica. Geophys. Environ. Eng. Probl.*, Las Vegas, Nevada, 10–14 February .

Manheim, F. T., D. E. Krantz, and J. F. Bratton (2004b), Studying ground water under Delmarva coastal bays using electrical resistivity, *Ground Water*, *42*(7), 1052–1068.

Martin, J. B., J. E. Cable, J. Jaeger, K. Hartl, and C. G. Smith (2006), Thermal and chemical evidence for rapid water exchange across the sediment water interface by bioirrigation in the Indian River Lagoon, Florida, *Limnol. Oceanogr.*, *51*(3), 1332–1341.

Martin, J. B., J. E. Cable, C. Smith, M. Roy, and J. Cherrier (2007), Magnitudes of submarine groundwater discharge from marine and terrestrial sources: Indian River Lagoon, Florida, *Water Resour. Res.*, *43*, W05440, doi:10.1029/2006WR005266.

Millham, N. P., and B. L. Howes (1994), Freshwater flow into a coastal embayment: Groundwater and surface water inputs, *Limnol. Oceanogr.*, *39*(8), 1928–1944.

Moore, W. S. (2006), The role of submarine groundwater discharge in coastal biogeochemistry, *J. Geochem. Explor.*, *88*, 389–393.

Mulligan, A. E., and M. A. Charette (2006), Intercomparison of submarine groundwater discharge estimates from a sandy unconfined aquifer, *J. Hydrol.*, *327*, 411–425.

Oberdorfer, J. A., M. A. Charette, M. Allen, J. B. Martin, and J. E. Cable (2008), Hydrogeology and geochemistry of near-shore submarine groundwater discharge at Flamengo Bay, Ubatuba, Brazil, *Estuarine Coastal Shelf Sci.*, *76*(3), 457–465.

Oliveira, J., W. C. Burnett, B. P. Mazzilli, E. S. Braga, L. A. Farias, J. Christoff, and V. V. Furtado (2003), Reconnaissance of submarine groundwater discharge at Ubatuba coast, Brazil using 222-Rn as a natural tracer, *J. Environ. Radioact.*, *69*, 37–52.

O'Rourke, D., (2000), Quantifying specific discharge into West Neck Bay, Shelter Island, New York, using a three-dimensional finite-difference groundwater flow model and continuous measurements with an ultrasonic seepage meter, M.Sc. thesis, 80 pp., State University of New York at Stony Brook, Stony Brook.

Paulsen, R. J. (1996), Analysis of the coastal groundwater/saltwater interface and continuous measurements of specific discharge into Coecles Harbor, Shelter Island, NY, M.Sc. thesis, 35 pp., State University of New York at Stony Brook, Stony Brook.

Paulsen, R. J., C. F. Smith, D. O'Rourke, and T. F. Wong (2001), Development and evaluation of an ultrasonic ground water seepage meter, *Ground Water*, *39*(6), 904–911.

Paulsen, R. J., D. O'Rourke, C. F. Smith, and T. F. Wong (2004), Tidal load and salt water influences on submarine groundwater discharge, *Ground Water*, *42*(7), 990–999.

Rapaglia, J. P. (2005), Submarine groundwater discharge into the Venice Lagoon, Italy, *Estuaries*, *28*(5), 705–713.

Saripalli, K., R. Khaleel, J. Serne, M. Lindberg, and K. Parker (2003), Tortuosity of immiscible fluids in porous media based on phase interfacial areas: A new definition and its application to Hanford's unsaturated media, *Abstracts with Programs* 35 (6), p. 482, *Geol. Soc. Am.*, September.

Schiavo, M. A., S. Hauser, G. Cusimano, and L. Gatto (2006), Geochemical characterization of groundwater and submarine discharge in the southeastern Sicily, *Cont. Shelf Res.*, *26*(7), 826–834.

Schlueter, M., E. Sauter, H. P. Hansen, and E. Suess (2000), Seasonal variations of bioirrigation in coastal sediments: Modeling of field data, *Geochim. Cosmochim. Acta.*, *61*(5), 821–834.

Seplow, M. S. (1991), The influences of groundwater seepage on the pore water salinity of Great South Bay, M.S. thesis, 80 pp., State University of New York at Stony Brook, Stony Brook.

Shaw, R. D., and E. E. Prepas (1989), Anomalous, short term influx of water into seepage meters, *Limnol. Oceanogr.*, *34*(7), 1343–1351.

Sholkovitz, E. R., C. Herbold, and M. A. Charette (2003), An automated dye-dilution based seepage meter for the time-series measurement of submarine groundwater discharge, *Limnol. Oceanogr.*, *1*, 16–28.

Smith, A. J., and S. P. Nield (2003), Groundwater discharge from the superficial aquifer into Cockburn Sound Western Australia: Estimation by inshore water balance, *Biogeochemistry*, *66*, 125–144.

Soren, J. (1978), Hydrogeologic conditions in the town of Shelter Island, in *USGS Water-Resources Investigations Report*, 77–77, 22 pp., Suffolk County Long Island, New York.

Stieglitz, T. (2005), Submarine groundwater discharge into the near-shore zone of the Great Barrier Reef, Australia, *Mar. Pollut. Bull.*, *51*, 51–59.

Stieglitz, T., P. V. Ridd, and S. Hollins (2000), A small sensor for detecting animal burrows and monitoring water conductivity, *Wetlands*, *8*, 1–7.

Stieglitz, T., J. Rapaglia, and S. Krupa (2007), An effect of pier pilings on near-shore submarine groundwater discharge from a confined aquifer, *Estuaries*, *30*, 543–550.

Stieglitz, T., M. Taniguchi, and S. Neylon (2008), Spatial variability of submarine groundwater discharge, Ubatuba, Brazil, *Estuarine Coastal Shelf Sci.*, *76*, 493–500.

Swarzenski, P. W., W. C. Burnett, W. J. Greenwood, B. Herut, R. Peterson, N. Dimova, Y. Shalem, Y. Yechieli, and Y. Weinstein (2006), Combined time-series resistivity and geochemical tracer techniques to examine submarine groundwater discharge at Dor Beach Israel, *Geophys. Res. Lett.*, *33*, L24405, doi:10.1029/2006GL028282.

Swarzenski, P. W., F. W. Simonds, T. Paulson, and S. Kruse (2007), A geochemical and geophysical examination of submarine groundwater discharge and associated nutrient loading estimates into Lynch Cove, Hood Canal, WA, *Environ. Sci. Technol.*, *41*, 7022–7029.

Taniguchi, M. (2006), Submarine groundwater discharge measured by seepage meters in Sicilian coastal waters, *Cont. Shelf Res.*, *26*(7), 835–842.

Taniguchi, M., and Y. Fukuo (1993), Continuous measurements of groundwater seepage using an automatic seepage meter, *Ground Water*, *31*, 675–679.

Taniguchi, M., and H. Iwakawa (2004), Submarine groundwater discharge in Osaka Bay, Japan, *Limnology*, *5*(1), 25–32.

Taniguchi, M., W. C. Burnett, J. E. Cable, and J. V. Turner (2002), Investigation of submarine groundwater discharge, *Hydrol. Processes*, *16*, 115–129.

Taniguchi, M., T. Ishitobi, and K. Seaki (2005), Evaluation of time-space distribution of submarine ground water discharge, *Ground Water*, *43*(3), 336–342.

Telford, W. M., L. P. Geldart, and R. E. Sheriff (1990), *Applied Geophysics*, 2nd ed., Cambridge Univ. Press, New York.

Ullman, W. J., and R. C. Aller (1982), Diffusion coefficients in nearshore marine sediments, *Limnol. Oceanogr.*, *27*(3), 552–556.

Urish, D. W. (1981), Electrical resistivity hydraulic conductivity relationships in glacial outwash aquifers, *Water Resour. Res.*, *17*(5), 1401–1408.

Vanek, V., and D. R. Lee (1991), Mapping submarine groundwater discharge areas-an example from Laholm Bay, Southwest Sweden, *Limnol. Oceanogr.*, *36*(6), 1250–1262.

Zhou, W., B. F. Beck, and J. B. Stephensen (2000), Reliability of dipole-dipole electrical resistivity tomography for defining depth to bedrock in covered karst terrains, *Environ. Geol.*, *39*(7), 760–766.

H. Bokuniewicz and J. Rapaglia, School of Marine and Atmospheric Science, 195 Endeavor Hall, Stony Brook University, Stony Brook, NY 11794-5000, USA. (john.rapaglia@gmail.com)

T. Stieglitz, School of Maths, Physics and IT, James Cook University, Townsville, QLD 4811, Australia.